An Investigation on the Crystal Growth Studies and Emission line shape in Er^{3+}-doped Sodium Tellurite Glasses

Purushottam Joshi*[1] and Animesh Jha

The Institute for Materials Research, Houldsworth Building, The University of Leeds, Leeds LS2 9JT, United Kingdom

[1]Formerly at the IMR, University of Leeds. Now at the Fibre Optics Laboratory, Raja Ramanna Centre for Advance Technology, Indore, India.

**E-mail: pjoshi@cat.emet.in*

Abstract: Crystallisation kinetics of the erbium doped soda-tellurite glasses were studied using the differential thermal analysis (DTA) and differential scanning calorimetery (DSC) techniques. The DTA curves in the temperature range of 350 K to 650 K were obtained from isochronal heating rates, chosen in the range of 2 to 20 K/min. DSC isothermal curves were used to calculate the fraction of crystals formed on reheating. The apparent activation energies for devitrification were derived by measuring the shifts in the values of T_g and T_x with heating rates, using the Kissinger method. The derived values of apparent activation energies for isochronal and isothermal methods varied in the range of 190-204 $\pm$ 5 kJ mol^{-1}. The X-ray powder diffraction analysis of heat treated and transparent samples showed the presence of nano-scale size sodium-tellurite crystals. These crystallites were found to have a strong influence on the full width of half maxima of the transition in Er^{3+}: $^4I_{13/2} \rightarrow {}^4I_{15/2}$, which extended from 70 nm in the vitreous materials to 132 nm in glass-ceramic materials.

1. Introduction

In the last decade efforts were made to broaden and flatten the overall bandwidth of erbium doped fibre amplifier, which in turn would increase the transmission capacity of wavelength-division-multiplexing (WDM) systems in the optical networks[1]. Mori et al[2] discussed different approaches for enhancing bandwidth of over 40 nm that is beyond the available bandwidth in Er-doped silicate fibre amplifiers. Amongst various techniques proposed, one of the techniques is based on the use of Er-ion as dopant in high-refractive index (n>1.9) tellurite glass as hosts, which offers multiple sites Er-ions and aids the line broadening to 80 nm. Tellurite glass fibre based Er-ion doped fibre amplifiers are therefore capable of providing seamless signal amplification with small-signal gains exceeding 20 dB over a bandwidth as wide as 80 nm, spanning across C- and L-bands from 1530 to 1610 nm[3].

The emission line shape and cross-section at a wavelength of the rare earth (RE) ions may be increased in glassy hosts by changing the ion environment from aperiodic glassy structure to a 3d-crystallites in the transparent glass-ceramic materials[4,5] while retaining the properties of the glassy matrix, which then suggests that a transparent glass-ceramic host may be able to provide a solution for a broadband and multi-channel optical amplification. However the main challenge in ensuring the transparency of such materials is in controlled nucleation followed by the limited growth rate of crystals formed in the glass matrix. For designing waveguides or fiber-based devices, characterization

* Corresponding Author: Purushottam. Joshi, Phone 0091 731 244 2327 E-mail: pjoshi@cat.ernet.in

of thermal stability and crystallization characteristics of tellurite-based glasses are essential. Crystal growth during reheating of glass preforms during fiber fabrication contributes to overall linear loss via light-scattering centers in the waveguide and, therefore negates any signal gain. In this paper we have investigated the overall kinetics of devitrification and analyzed the crystal growth properties for making a transparent glass-ceramic composite for light amplification[6]. This paper also explains how controlled crystallization increases emission cross-sections of the Er^{3+} ion while retaining transparency of glass.

2. Experimental

The sodium tellurite glass compositions in the range of: $\{XNa_2O\text{-}(100\text{-}X)TeO_2\}_{1-y}$ $(Er_2O_3)_y$ (where X = 5 to 25) were prepared according to the following procedure. High-purity oxides (99.999% and 99.99% pure) were batched and weighed using the constituent oxides molar masses and percentages and then mixed. Each mixture of powders was heated in a furnace at temperatures ranging from 1000 to 1100 K depending on the melting properties of each composition. The melted bath was then kept under a flow of dry oxygen gas passed at 1.5 LPM (liter per minute). After this treatment, the melts were cast into mould preheated at the glass transition temperature and the solids were annealed at this temperature for 2 h before being cooled down slowly to room temperature with a cooling rate of 0.25 K min^{-1}. The glass sample was cut to have 5 mm x 5 mm x 2 mm size. The glass samples were heat treated at various temperatures from glass transition to crystallization temperature with different soaking time. Isothermal and non-isothermal measurements were done using Perkin-Elmer Differential Scanning Calorimeter 7 (DSC) and Differential Thermal Analyzer (DTA) respectively. For isothermal runs small amount of glass samples weighing 20-30 mg were placed inside baked alumina powder to provide a very good thermal contact. The sample was then heated at a rate from 10 K per minute under a purge of nitrogen gas maintained at a rate of 250 ml min^{-1}. For non-isothermal runs, the glass samples were heated at a number of heating rate between 2 and 30 K per minute. In case of DSC scans, each sample was hermetically sealed inside an aluminium pan and heated to near crystallization temperature rapidly (500 K min^{-1}) and then held for 20 minutes allowing for crystal growth to occur.

Emission measurements were taken using a 5 watt Innova Coherent Argon ion (Ar^+) laser, a Titanium Sapphire ($Ti:Al_2O_3$) laser (Schwartz Electro Optic, model CWBB, Orlando, Florida), driven by two 5 watt Ar^+ lasers(Coherent model Innova 90, Santa Clara, California). The Argon ion laser emits at 488 nm, whilst the Ti:Sapphire laser is a continuous wave (CW) type in which the strongest emission bands is between 710 nm and 870 nm. In this study, we used the 800 nm wavelength as the excitation source. These lasers were used to excite ions in the glass samples, which were positioned in the pump beam in order to obtain a long path length. The fluorescence spectrum from the sample was recorded by the fluorescence spectrometer (Edinburgh Instruments model FS 920, Livingston, UK), for which the InxGaa-xAs detector was used for the near-infrared range emission between 1450 and 1700 nm.

3. Results and Discussions:

The glass transition temperature (T_g), corresponds to a temperature range near which the viscosity may correspond to $10^{12} \sim 10^{13}$ Pa s. The physical changes in the glass in this temperature corresponds a transformation from a solid-like to a liquid-like behaviour. The onset of crystallization (T_x) indicates the temperature range in which the glass viscosity is sufficiently low to permit rapid crystal growth. T_x is plotted by extrapolating onset of the first crystallization exotherm, as shown in Fig. 1 From a DSC or DTA scan, the $T_x - T_g$ gap can be calculated which is a rough estimate of glass stability on reheating, and is considered to be an important indicator for estimating the fibre drawing range of a glass without encountering major crystallization. For fibre drawing, a low enough viscosity ($\approx 10^{4.5}$ Pa s) must be exhibited in this temperature region. Therefore, this gap should be maximized so that the glass fibres exhibit low optical absorption and scattering losses. However, for a glass to have a fibre drawing viscosity of $\sim 10^{4.5}$ Pa s well below its T_x, a large T_x-T_g gap must be exhibited corresponding to a shallow viscosity-temperature relationship, i.e. a non-fragile glass-forming liquid like behaviour, argued by Angell[7].

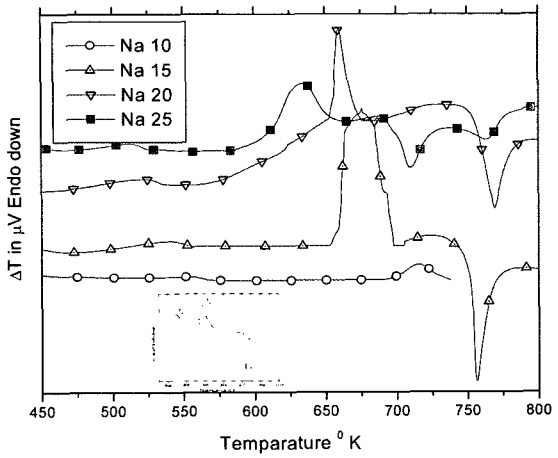

Fig. 1. DTA trace of glass (100-X)TeO_2 -X Na_2O for X= 10 to 25 when heated with 10 K/min Inset at left bottom showing schematic representation of characteristic temperatures.

Fig. 1 shows the DTA traces of glasses (100-x) TeO_2 – x Na_2O where x ranges between 10 and 25 mole percent. The inset shown in figure illustrates the characteristic temperatures of thermal analysis peaks. The first endotherm at around 550 K is the glass transition temperature (T_g). The onset of this temperature is obtained by interpolating the straight line just before the transition and the straight line that occurs after the initial change. The first exotherm in Fig. 1 at around 670 K is due to a crystallization event in the glass. The onset of crystallization, T_x, is obtained by plotting the 'lift-off' point from the baseline where slope begins to change. The peak temperature of a crystallization exotherm and melting temperature are designated by T_p and T_m, respectively. Irreversible transformations are those in which reactants do not reform from the products on cooling. Here one of the reactant is a metastable state (i.e. glass) and only requires heat to raise it above T_g to the under cooled liquid state to initiate the transformation. Devitrification of glass is a classic example of an irreversible transformation. In such a type of reaction, the sample temperature does not remain constant during the transformation. As the glass devitrification proceeds, heat released at the glass-crystal interface raises the temperature of the sample. The rates of such transformations generally have an exponential temperature dependence, causing them to proceed more rapidly, which in turn raises temperature further, and so on.

Table 1 summarizes the characteristic temperature of tellurite. T-90 has the highest glass transition temperature and a large $T_x - T_g$ gap, indicating that the nucleation may be slow due to the exponential dependence on ΔT, which is why we chose this glass for heat treatment studies. However, the lowest value of ΔT_p means that once the crystals are formed, they grow rapidly due to a large overall transformation.

Three different conditions can be considered based on the empirical observation of T_x-T_g and T_m-T_x or T_m-T_p and explain the overall crystallization tendency of glasses described in Fig. 1.

$$\Delta T = (T_x - T_g) \quad \text{difference,} \tag{1}$$

$$S = \frac{\Delta T(T_p - T_x)}{T_g} = \frac{\Delta T_p}{T_g} \quad \text{parameter, and} \tag{2}$$

$$H_R = \frac{(T_x - T_g)}{T_m - T_x} = \frac{\Delta T}{\Delta T_m} \quad \text{ratio.} \tag{3}$$

3.1 Non-isothermal crystallization:

A typical DTA curve for a TeO_2 glass sample obtained at a heating rate of 10 K min^{-1} is shown in Fig. 1, where T_g is the glass transition temperature, T_x is the onset temperature of crystallization, and T_p is the peak of exothermal crystallization. Due to the dependence of glass crystallization on time, the crystallization peak

Table 1. A comparison of Characteristic Temperatures of Sodium Tellurite Glasses and Their Thermal Stability Parameters, Determined by DTA

Sample	Compositions, mol%	T_g, K	T_x, K	T_p, K	T_m, K	ΔT, K	H_R,	S, K	ΔT_p K	ΔT_m K
T-95	TeO_2-95, Na_2O-5	562	665	670	963	103	0.35	0.92	5	293
T-90	TeO_2-90, Na_2O-10	563	690	708	918	127	0.56	4.06	18	210
T-85	TeO_2-85, Na_2O-15	551	662	679	823	111	0.69	3.42	17	144
T-80	TeO_2-80, Na_2O-20	535	649	661	743	114	1.21	2.56	12	82
T-75	TeO_2-75, Na_2O-25	523	620	630	733	97	0.86	1.85	10	103

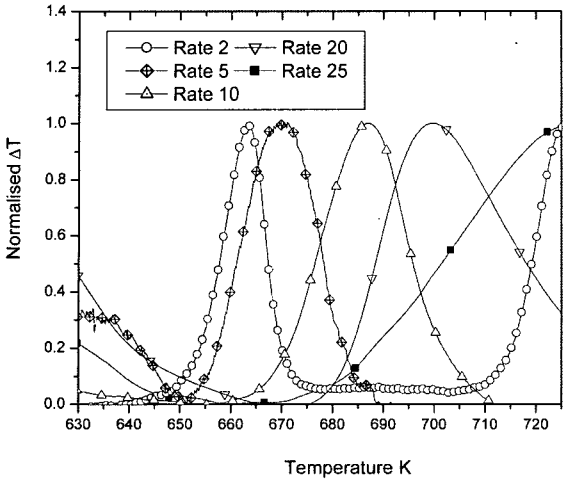

Fig. 2. The normalised crystallisation peaks for glass $90TeO_2$ -$10Na_2O$ with various heating rates in K/min.

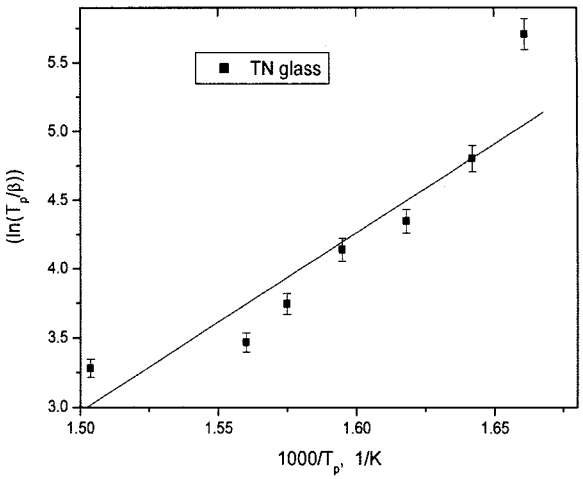

Fig. 3. $\ln(T_p/\beta)$ v/s$1000/T_p$ for glass $90TeO_2$ -$10Na_2O$.

position shifts to higher temperatures as the heating rate increases. The normalized crystallization peaks (T_p) of $10Na_2O$-$90TeO_2$ are shown in Fig. 2 for various heating rates determined from DTA curves. Since the DTA could not be used at higher heating rate than 25 K min^{-1}, we were unable to extend the temperature range of measurements. On the other hand the DSC could have been used, but in our experience we have found that even hermetically sealed tellurite glass attacks the DSC cell by contaminating platinum holder.

On the basis of the *J-M-A* equation[8], Ozawa[9] and Chen[10] proposed a method, which enables the determination of the value of activation energy (E_c) from the shift in the devitrification peak (T_p) position as a function of isochronal heating rate (β) in accordance with the Kissinger method[11]:

$$\ln\left(\frac{T_p}{\beta}\right) = \frac{E_c}{RT_p} + \left(\frac{1}{n}\right)\left[\ln\left(-\ln(1-x)\right)\right] - \ln\left(\frac{k_0}{2}\right) \qquad (4)$$

Using equation 4, the overall activation energy E_c can be determined either at x=0, i.e. the onset of devitrification or at x=0.5. This equation is also useful for analyzing whether the overall devitrification peak is a convolution of one or more thermal events by taking the derivative of the term, $\ln\left[\frac{T_p}{\beta}\right]$ with respect to x, along the devitrification exotherm. In order to acquire the value of the activation energy of the crystallization, a linear relationship between $\ln(T_p/\beta)$ and $1000/T_p$ was plotted in Fig. 3, from which activation energy, E_c, for the tellurite based glasses can be calculated using equation 4, which are tabulated below.

The formation of critical nucleus can be explained using classical theory for nucleation applicable in three conditions[12]. Under condition 1, Gibbs volume free energy ($\pi r^3 \Delta G_{v1}$) changes steeply. As $\Delta T_m = T_m - T_x \equiv T_x - T_g$ are small crystal radius (r_1*) and change is Gibbs free energy (ΔG_1*)is also small. ΔT_m gives rough estimate of metastable crystal., which grows further cyrstallisation process. The value of n (= 2.49) means that the surface nucleation and one-dimensional growth are dominant for metastable crystals formed at T_x. Since T_m-T_x is the largest for T-95 glass, this explains that the metastable crystals have the largest value for the Gibbs energy of crystallization. The resultant ΔG_1* and r_1* mean that once the nucleation begins, the growth rate will increase at least at a rate of $[(T_m-T_x)]/T$[13].

Under the condition 2, the surface energy term is considered same as in condition 1, except the T_m-T_x differential is smaller. Consequently the ΔG_2* curve has a smaller curvature compared to curve condition 1, which when added together with surface energy (same as in condition 1) yields ΔG_2* and r_2*, both of which are larger than those described under condition. For T-90 glass the T_m-T_x gap is much smaller than in T-95. The condition 3 represents a case where T_m-T_x may be

not only much smaller than in either condition 1 and 2, but also T_x-T_g may also be much larger than the conditions 1 and 2, discussed above. The presence of a broad and small crystallization peak for glass is a clear evidence for much reduced surface crystallization and one-dimensional crystal growth, which might not be occurring because the breadth of the crystallization peak. The corresponding change in Gibbs free energy curve will have shallower shape of cubic parabola. The absence of exotherm reflects that ΔT and ΔT_m are likely to have the largest and smallest values. On the basis of classical explanation, therefore, we may be able to propose the magnitudes of critical radius compared in a following ascending order.

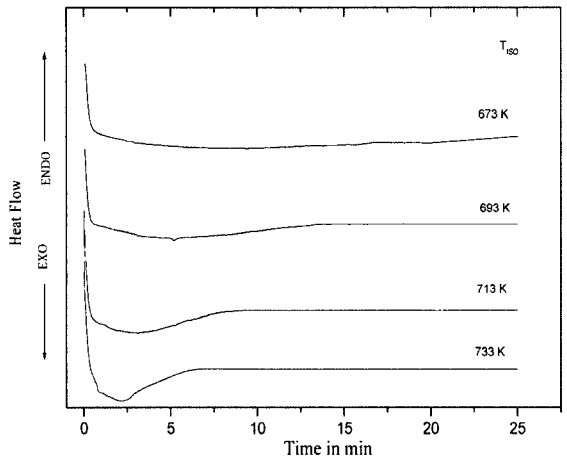

Fig. 4. Isothermal traces for glass $90TeO_2$ -$10Na_2O$ using DSC.

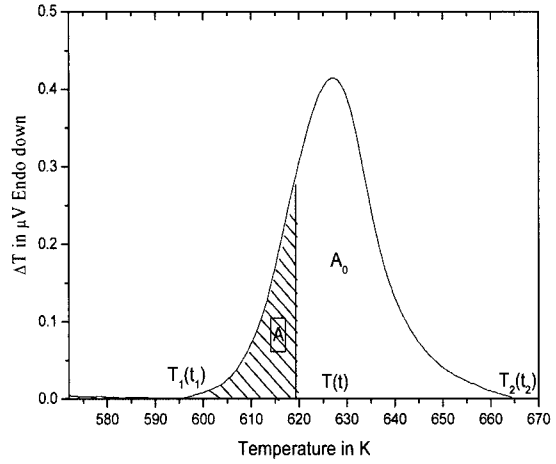

Fig. 5. Volume fraction of crystallised at time t.

3.2 Isothermal Crystallization

The data for isothermal crystallization are recorded in the temperature range from 670 to 740 K using DSC and curves are shown in Fig. 4. The volume fraction of crystallized x, crystallized at time t was determined from the ratio of the area under the crystallization exotherm up to time t to the total area, as shown in Fig. 5 The values of the volume fraction crystallized, x are plotted against time, t in minute for the glasses in Fig. 6. From linear plots of ln(-ln(1-x)) against ln (t, sec) as shown in Fig. 7. The values of n (a dimensionless exponent) and *k* (the rate constant) are derived by calculating slope for the linear fit and substituting values in the following equation

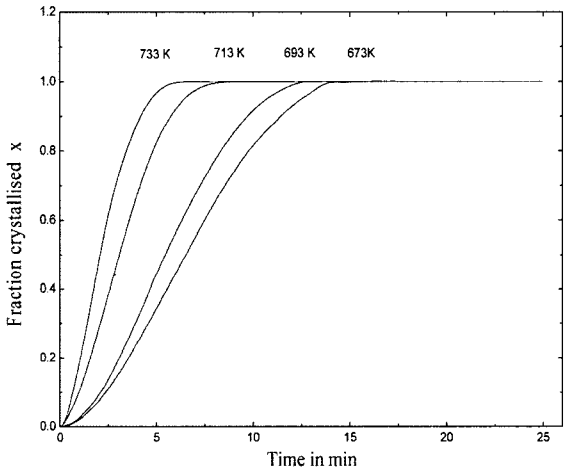

Fig. 6. Fraction crystallized as function of time in $90TeO_2$ - $10Na_2O$.

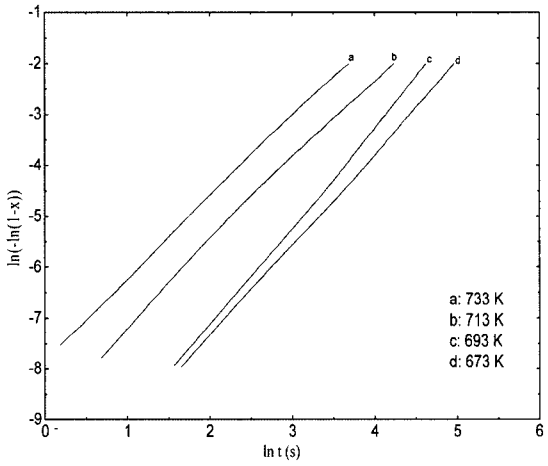

Fig. 7. JMA equation plots for isothermal crystallisation for glass $90TeO_2$ -$10Na_2O$.

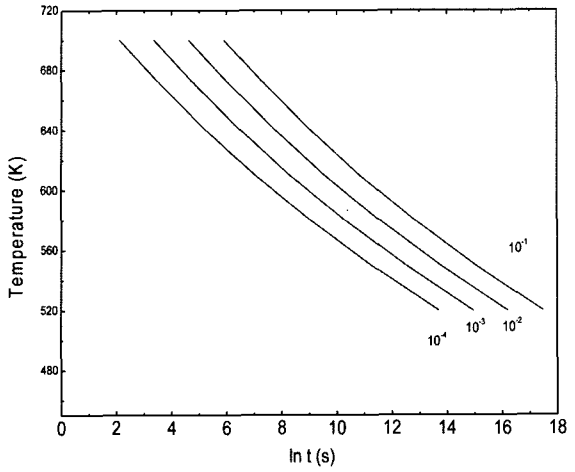

Fig. 8. TTT plots for different values of fraction crystallised for glass $90TeO_2$-$10Na_2O$.

$$\ln [- \ln (1-x)] = n \ln k + n \ln t \quad (5)$$

The activation energy E_c is calculated using

$$\ln k = \ln k_0 - E_c/RT \quad (6)$$

where R is the universal gas constant.

$$\ln t_m = -0.367/n - \ln k_0 + E_c/RT \quad (7)$$

t_m is the exotherm maximum t_m the volume fraction crystallized x. The values of n, k and E_c are tabulated in table 2.

The derived values of *n*, in general, indicate the mechanism of glass devitrification: n = 1 surface nucleation, n = 2 one dimensional bulk growth and n = 3 two dimensional bulk growth. The values of n for tellurite-based glasses are less than 2, as is shown in table 2, which suggest that the mechanism of devitrification in these glasses is based on the surface nucleation and one dimensional crystal growth[14,15]. A prerequisite for glass formation from the liquid state is that the cooling be sufficiently fast to preclude crystal nucleation and growth, since the crystalline phase is thermodynamically more stable and, the crystal growth will always dominate over the formation of the glass if allowed to take place. From table 2, the temperature dependence of the rate constant k was derived for the binary compositions, from the Arrhenius equation 4:

$$\ln k = 3.3 - \frac{5600}{T} \quad (8)$$

Using the above values of n and k, we have computed the partial time-temperature-transformation (*t-t-t*) curves for binary glasses for $x = 10^{-1}$ *to* 10^{-4}, which are compared in Fig. 8.

3.3 Fluorescence properties of heat-treated Er-doped sodium tellurite and X-ray diffraction data

Fig. 9 shows emission spectra of Er^{3+} ion in TeO_2-90, Na_2O-10 glass. NHT is the as is glass, whereas the rest are the heat treated at respective temperatures for 10 h. We observed that above 623 K, the samples were

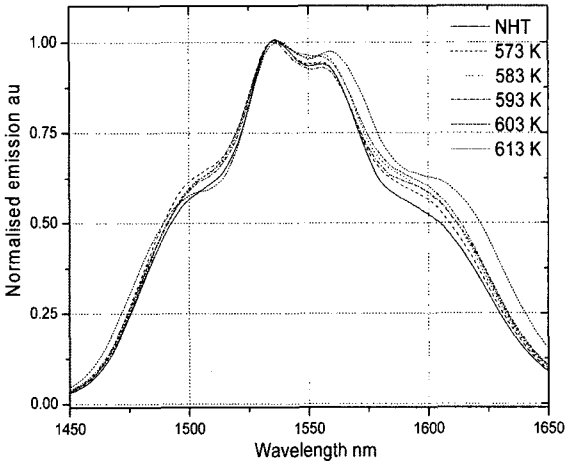

Fig. 9. Er^{3+} ion emission spectroscopy for heat treated sodium tellurite {$0.005Er_2O_3$ 0.995 [Na_2O-10, TeO_2-90] glass for 10 h. NHT is a glass without heat treatment.

Table 2. Comparison of the Values of Activation Energy Ec, Avrami Exponent n, and Rate Constant k of Devitrification of Binary Sodium Tellurite Glasses, Determined from Equations (4), (6) and (7)

Glass	Equation 4				
	n ± 0.1	ln (k_0) s^{-1} ± 4		E_c kJ/mol ± 5	
$90TeO_2$ -$10Na_2O$	2.49	48		204	
Glass	n ± 0.1	Equation 6		Equation 7	
		ln (k_0) s^{-1} ± 2	E_c kJ/mol ± 4	ln (k_0) s^{-1} ± 2	E_c kJ/mol ± 4
$90TeO_2$ -$10Na_2O$	1.76	26	191	29	190

opaque to the naked eye, it is for this reason all comparisons for emission line broadening were made below 623 K. An increase in the cross-section of the emission of Er^{3+} ion is expected due to the changing electric dipole environment from glass to a sub-micro to microsrytsalline state crystalline state[6] while retaining the properties of the glassy matrix. Hence glass-ceramic systems could be a promising solution for a broadband amplifier, provided that they remain optically isotropic and transparent. The crucial problem in getting such materials is the nucleation of the starting glass and the way to initiate it, and afterwards to control the crystal growth of the particles in order to keep the transparency of the system. The emission measurements of the heat treated erbium doped sodium tellurite glasses are very similar in shapes, although they slightly varied in intensity. We also observed changes in the area of peak. Broadening of the emission mainly depends on the distribution of the sites of Er^{3+} ion in the glass as well as the interaction of the Er^{3+} ions with the nearby dipoles. In our measurements, the effects of sample size, detector position and other extraneous factors which artificially broaden the Er spectra were excluded by optimizing the experimental condition.

Since the glass-ceramics have both short-range and longer range orders because of the presence of micro- and nanoscale crystallinity, we expect the contributions to electric and magnetic dipole to change in the vicinity of Er-ions in the glass and crystals. Ligand fields which include electric dipole and magnetic dipole govern the spectral broadening. 0.995 (10 Na_2O 90 TeO_2) - 0.005Er_2O_3 glasses are heat treated near glass transition temperature. Zhu el al[16] suggested the formation of new Na_2O 8 TeO_2 (NT_8) crystals when the sodium tellurite glass is heat treated above 600 K. The X-ray diffraction of these glasses confirms the presence of sodium tellurite crystallites, as shown in Fig. 10.

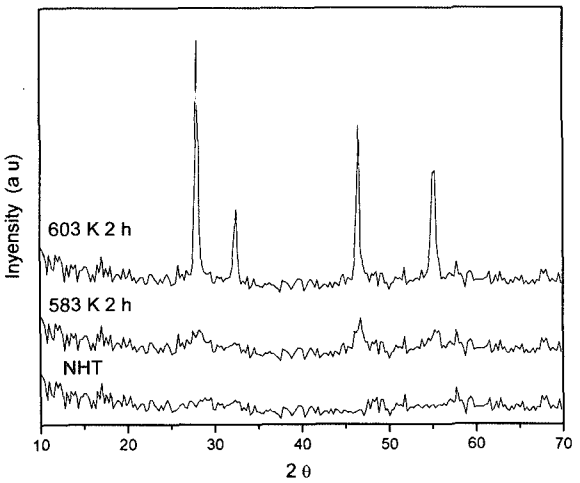

Fig. 10. XRD for 10 Na_2O 90 TeO_2 glass crystallized at 603, 583 K for 10 h and not heat treated (NHT) samples. 603 K sample showing Na_2O 8TeO_2 crystal[16].

4. Conclusions

Crystallization kinetics of the (XNa_2O 100-$XTeO_2$) glasses were studied and the overall activation energies for the crystallization processes were determined to be in the range of 190-204 kJ mol^{-1} in the temperature range 670 to 740 K. The crystallized phases formed upon heat treatment of these glasses were identified by XRD. The partial *t-t-t* curves were derived from the JMA analysis. A new Na_2O 8 TeO_2 (NT_8) crystal phase was observed when the sodium tellurite glass was heat treated above 600 K. Controlled heat treatment of sodium tellurite glass yielded transparent glass-ceramics which exhibit the effects of line broadening from 80 nm to 130 nm.

Acknowledgements

PJ acknowledges the financial assistance from the Overseas Research Scholarship office from the University of Leeds. The authors acknowledge the support from the Engineering and Physical Science Research Council under research grant GR/R31454/01.

References

1. J. F. Massicott, J. R. Armitage, R. Wyatt, B. J. Ainslie, and S. P. Craig- Ryan, *Electron. Lett.*, 26, 1645-1646, (1990)
2. A. Mori, T. Sakamoto, K. Kobayashi, K. Shikano, K. Oikawa, K. Hoshino, T. Kanamori, Y. Ohishi, and M. Shimizu, J Lightwave Tech. 20, 5, 794-799 (2002)
3. A. Mori, Y. Ohishi, M. Yamada, H. Ono, Y. Nishida, K. Oikawa, and S. Sudo, *OFC'97.*, 1997, Paper PD1.
4. C.F. Rapp, and J. Chrysochoos, J. Mater. Sci., 7, 1090 (1972).
5. F. Auzel, D. Pecile, and D. Morin, J. Electrochem Soc.,

122, 101 (1975).
6. S. W. Martin and C. A Angell. J of Phy. Chem., 90, 6736-6740 (1986)
7. C. A. Angell, J Non-Crys., Solids, 73, 1-17, (1985)
8. M. Avrami, J. Chem. Phys. 7, 1103, (1939); 8, 212 (1940); 9 177 (1941)
9. T. Ozawa, Bull. Chem. Soc. 38, 1 1881 (1965)
10. S. H Chen, J. Non-Crystalline. Solids 27, 257 (1978)
11. H. E. Kissinger, Anal. Chem. 29,1702 (1957)
12. X. Liu, S. Shen., and A. Jha, J. Mater. Res., 20, 4, 857, (2005)
13. W.D. Kingery, H.K. Bowen, and D.R.Uhlmann, 'Phase transformation, glass formation, and glass ceramics' in Introduction to Ceramics, 2nd ed. (John Wiley and Sons, 340-345. (1976)
14. V D. Fedorov, V V. Sakharov, A M. Provorova, P B. Baskov, M F. Churbanov, V S. Shiryaev, Ma Poulain, Mi Poulain, and A Boutanfaia., J. Non-Cryst. Solids 284, 79 (2001)
15. P. W. Atkins, Physical Chemistry, 5th ed. Oxford: Oxford University Press, (1994)
16. D. Zhu, W. Zhou, and C. S Ray., J of Mat. Res., 20, 1961-63. (2001)